Hindawi

Research Article

Radiative Flow of Copper and Aluminum Nanoparticles with Heat Source Phenomenon: Dual Numerical Simulations and Stability Analysis

Sumera Dero,[1] Liaquat Ali Lund,[2] Al-Khaled Kamel [iD],[3] Asjad Muhammad Imran [iD],[4] Taseer Muhammad [iD],[5] Sami Ullah Khan,[6] and A Abbasi[7]

[1]*Institute of Mathematics and Computer Science, University of Sindh, Jamshoro, Pakistan*
[2]*KCAET Khairpur Mirs, Sindh Agriculture University, Tandojam, Sindh 70060, Pakistan*
[3]*Department of Mathematics & Statistics, Jordan University of Science and Technology, P.O. Box 3030, Irbid 22110, Jordan*
[4]*Department of Mathematics, University of Management and Technology, Lahore, Pakistan*
[5]*Department of Mathematics, College of Science, King Khalid University, Abha 61413, Saudi Arabia*
[6]*Department of Mathematics, COMSATS University Islamabad, Sahiwal 57000, Pakistan*
[7]*Department of Mathematics, University of Azad Jammu and Kashmir, Muzaffarabad 13100, Pakistan*

Correspondence should be addressed to Taseer Muhammad; taseer_qau@yahoo.com

The thermally developed flow of nanoparticles due to bidirectional moving space has been presented numerically. The additional impact of heat source and sink are also incorporated for enhancing the heat transfer rate. The copper and aluminum nanoparticles are selected for enhancing the thermal diffusion system. The thermal stability of nanoparticles is carefully addressed. The moving surface allows the shrinking and stretching phenomenon. The system of resulting equations with nonlinear nature is numerically swapped via shooting technique with help of MATLAB software. The dual numerical simulations for the thermally radiative problem with external heating phenomenon are being performed. It is noted from results that thermal stability of nanoparticles is more stable in the upper branch of shrinking/stretching surface. The presence of heat source provides extra heat and improves the thermal transportation phenomenon which is more progressive in upper branch. The enhancement in temperature profile due to copper nanoparticles is more stable as compared to aluminum nanoparticles. Moreover, the increasing change in the velocity is resulted upon increasing the rotation constant. The obtained results reflect applications in thermal sciences, heating systems, energy production, solar applications, nuclear reactions, biomedical applications, etc.

1. Introduction

Recently, motivations of researchers are noticed towards the nanofluid which reports leading contributions in the thermal engineering and industrial processes. The growing interest in nanomaterials is justified due to highly attractive applications in solar energy, thermal transportation systems, engineering devices, cooling systems, heating objectives, nuclear reactions, medical sciences, emission processes, etc. With nanostructured (1–100 nm), the nanofluids report excellent thermal activities. The interaction between nanoparticles and some base fluids reports results enhanced thermal mechanism of base fluids. Choi [1] focused first time

on the thermal aspect of nanofluids via experimental approach. Later on, diverse research is being performed by investigators to highlight the thermal mechanism and applications of nanomaterials. Turkyilmazoglu [2] developed a slip nanofluid model for the annuli flow by utilizing the dual nanofluid and single relations of the nanofluid model. Nayak et al. [3] exploited the viscous dissipation consequences for illustrating the nanofluids flow with Oldroyd-B base material via bidirectional space. Basir et al. [4] performed the novel aspect of slip flow of nanofluid with sensitivity insurance and bioconvection phenomenon. The Maxwell nanofluid thermal determinations subject to the interaction of multiple types of slip consequences have been identified

by Ahmad et al. [5]. The Buongiorno nanofluid model implementation for inspecting the viscoelastic fluid thermal capacity was reported in the work of Nadeem et al. [6]. The analytical simulation for the nanofluid Riga surface problem was investigated by Vaidya et al. [7]. Wang et al. [8] focused on the migration of nanofluid material minichannels having parallel plates. Abdelaziz et al. [9] discussed the characteristics of nanofluid pattern via horizontal tubes. The continuation of Sabu et al. [10] determined the heat transfer improvement for the alumina nanoparticles with slip constraints due to heated rotatory disk. Ojjela et al. [11] addressed the viscoelastic behavior and thermal capability for the nanoparticles with non-Newtonian base fluid. The stability determination of nanofluids with experimental approach was determined by Dong et al. [12]. Sivasankaran and Bhuvaneswari [13]investigated the heat transfer mechanism with constraints of pressure loss and porous space. Acharya [14] numerically focused on the natural convective flow of nanofluid due to heated wall surface in square enclosure. Mondal et al. [15] addressed the optimized thermal mechanism due to the couple stress nanofluid with radiative phenomenon. Acharya [16] discussed the finite element numerical simulations for the spinning flow of nanoparticles with active and passive control approach. Shafiq et al. [17] addressed the bioconvection aspect of nanofluid with zero mass constraints. Haya et al. [18] addressed the Joule heating effects while inspecting the enhanced aspect of heat transfer in third grade nanofluid. Some more recent work on nanofluid flow is presented in [19–24].

The hybrid nanofluid is the modified form of nanofluids with more improved thermal activities. In fact, the hybrid nanofluid model is based on the interaction of more than one different types of nanoparticles along with base material. The preferences of the hybrid nanofluid model over simple nanomaterials are due to extra high activities and more thermal stability. Recently, different investigations are performed on hybrid nanofluid with different nanoparticles. Sowmya et al. [25] reported the inclusion of iron nanoparticles with existence of Lorentz force in cavity with two heated fins. Sundar et al. [26] claimed the hybrid nanofluid thermal properties with collector applications. Akhtar et al. [27] modeled a hybrid nanofluid problem in elliptic duct following the peristaltic mechanism. Eid and Mabood [28] noticed the ethylene glycol base fluid thermal inspection with hybrid nanofluid numerically. Eid and Mabood [28] presented the thermal research on the carbon nanotubes flow with heat generation features. Shahid et al. [29] implemented the Darcy porous law for studying the hybrid nanofluid prospective in parabolic surface. Madhukesh et al. [30] explored the thermal efficiencies of AA7072-AA7075 nanoparticles with Newtonian heating enrollment. Acharya [31] discussed the shape characteristics for the hybrid nanofluid in heated obstacles. Devi and Devi [32] visualized the copper and aluminum oxide nanoparticles thermal prospective accounted via stretching surface. Devi and Devi [33] observed the 3D thermal flow problem with Newtonian heating. Lund et al. [34] intended the rotating flow of hybrid nanofluid. Teh and Ashgar [35] determined the Joule heating

for the rotating flow of hybrid nanofluid. Zaimi et al. [36] discussed the multiple solution of rotating viscoelastic fluid with hybrid nanofluid.

This analysis deals with the impact of heat source and thermal radiation effects in flow of hybrid nanofluid due to rotating space. The main motivation for performing this investigation is to highlight the enhanced thermal aspect of heat transfer phenomenon subject to the magnetized copper and aluminum nanoparticles. The moving surface attained the stretching and shrinking phenomenon. The thermal stability of hybrid nanoparticles is focused. The shooting numerical algorithm is followed for the simulations process. The dual simulations are performed in each branch of moving space.

2. Problem Formulation

The stretching and shrinking phenomenon of 3D hybrid nanofluid is taken into account. The heat transfer analysis is considered in presence of external heating source and thermal radiation. The magnetic force impact is directed along the z-axis for 3D flow. The three-dimensional moving space attained the velocity $u_w(x) = \lambda c x^n$. The stretching and shrinking results are attained for $\lambda > 0$ and $\lambda < 0$, respectively. The surface temperature of nanoparticles is notified with T_w while T_∞ is for free stream temperature case as shown in Figure 1. The nanoparticles and surface present rotatory behavior with angular velocity $\widetilde{\Omega} = \Omega_0 x^{(1-n)}$ along z-direction. Let u, v, and w be representation of velocities along , y, and z directions, respectively. The assumptions of low magnetic Reynolds number reduce the role of induced magnetic force. The governing relations in view of such considerations are as follows [26–28]:

$$u_x + v_y + w_z = 0, \tag{1}$$

$$uu_x + vu_y + wu_z - 2\widetilde{\Omega}v = -\frac{P_x}{\rho_{hnf}} + \frac{\mu_{hnf}}{\rho_{hnf}}\left[u_{xx} + u_{yy} + u_{zz}\right]$$
$$- \frac{\sigma_{hnf}}{\rho_{hnf}}B^2 u. \tag{2}$$

$$uv_x + vv_y + wv_z + 2\widetilde{\Omega}u = -\frac{P_y}{\rho_{hnf}} + \frac{\mu_{hnf}}{\rho_{hnf}}\left[v_{xx} + v_{yy} + v_{zz}\right]v$$
$$- \frac{\sigma_{hnf}}{\rho_{hnf}}B^2 v, \tag{3}$$

$$uw_x + vw_y + ww_z = -\frac{P_z}{\rho_{hnf}} + \frac{\mu_{hnf}}{\rho_{hnf}}\left[w_{xx} + w_{yy} + w_{zz}\right], \tag{4}$$

$$\left(\rho c_p\right)_{hnf}\left[uT_x + vT_y + wT_z\right] = k_{hnf}\left[T_{xx} + T_{yy} + T_{zz}\right]T$$
$$- q_{r\,z} + Q_0\left(T - T_\infty\right). \tag{5}$$

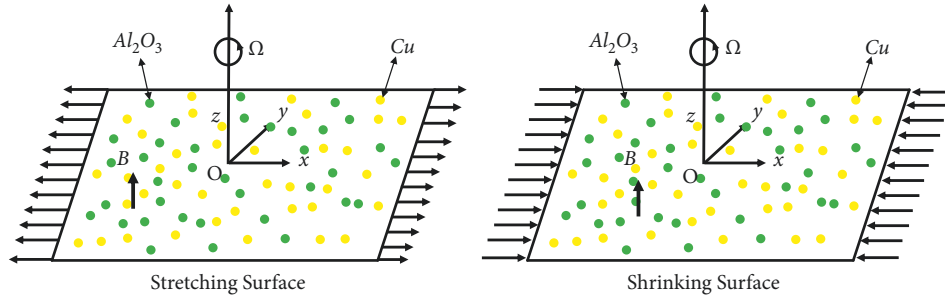The related boundary conditions are as follows:

FIGURE 1: Flow illustration of problem.

$$\begin{cases} w = w_w(x), v = 0, u = u_w(x), T = T_w \text{ at } z = 0 \\ u \longrightarrow 0, v \longrightarrow 0, T \longrightarrow T_\infty \text{ as } z \longrightarrow \infty \end{cases} \quad (6)$$

The relation for radiative flux q_r is given by $q_r = -(4\sigma^*/3k^*)(\partial T^4/\partial z)$. Table 1 and Table 2 provide the thermophysical properties.

The following similarity variables (7) are used to obtain similarity solutions for equations (1)–(5):

$$\begin{cases} u = cx^n f'(\eta), v = cx^n g(\eta), \eta = z\sqrt{\dfrac{c(n+1)}{2\vartheta_f}} x^{(n-1)/2} \\ \\ w = -\sqrt{\dfrac{c\vartheta_f(n+1)}{2}} x^{(n-1)/2} \left[f(\eta) + \dfrac{n-1}{n+1}\eta f'(\eta) \right] \\ \\ \theta(\eta) = (T - T_\infty)/(T_w - T_\infty) \end{cases} \quad (7)$$

The dimensionless set of equation is

$$f''' + \xi_1 \xi_2 \left[ff'' - \frac{2n}{(n+1)}f'^2 + \frac{4\Omega}{(n+1)}g \right]$$
$$- \frac{2}{(n+1)}\frac{\sigma_{hnf}}{\sigma_f}\xi_2 M f\prime = 0, \quad (8)$$

$$g'' + \xi_1 \xi_2 \left[fg' - \frac{2n}{(n+1)}f'g - \frac{4\Omega}{(n+1)}f' \right]$$
$$- \frac{2}{(n+1)}\frac{\sigma_{hnf}}{\sigma_f}\xi_2 Mg = 0, \quad (9)$$

$$\frac{\xi_3}{Pr}\left(\frac{k_{hnf}}{k_f} + \frac{4}{3}R\,d \right)\theta'' + \theta' f + \xi_3 Q\theta = 0, \quad (10)$$

subject to BCs,

$$\begin{cases} f(0) = -b\sqrt{\dfrac{2}{n+1}}, f'(0) = \lambda, g(0) = 0, \theta(0) = 1 \\ \\ f'(\eta) \longrightarrow 0, g(\eta) \longrightarrow 0\ \theta(\eta) \longrightarrow 0,\ as\ \eta \longrightarrow \infty \end{cases},$$

$$\begin{cases} \xi_1 = \left\{ (1 - \phi_{Cu})\left[1 - \phi_{Al_2O_3} + \phi_{Al_2O_3}\left(\dfrac{\rho_{Al_2O_3}}{\rho_f} \right) \right] + \phi_{Cu}\left(\dfrac{\rho_{Cu}}{\rho_f} \right) \right\} \\ \\ \xi_2 = (1 - \phi_{Cu})^{2.5}(1 - \phi_{Al_2O_3})^{2.5} \\ \\ \xi_3 = \dfrac{1}{\left\{ (1 - \phi_{Cu})\left[1 - \phi_{Al_2O_3} + \phi_{Al_2O_3}(\rho c_p)_{Al_2O_3}/(\rho c_p)_f \right] + \phi_{Cu}(\rho c_p)_{Cu}/(\rho c_p)_f \right\}} \end{cases}, \quad (11)$$

where prime "$\prime$" denotes the differentiation by η, $M = (\sigma_f B_0^2/c\rho_f)$ is the magnetic number, $Pr = (\vartheta_f/\alpha_f)$ is Prandtl, $\Omega = (\Omega_0/c)$ is rotation parameter, Q shows the heat source/sink parameter, and $R\,d = (4\sigma^* T_\infty^3/k^* k_f)$ denotes the thermal radiation constant and b suction ($b > 0$)/injection ($b > 0$) constant.

The dynamic of local Nusselt number and skin friction coefficient is

$$C_{fx} = \frac{\mu_{hnf}}{\rho_f u_w^2}\left(\frac{\partial u}{\partial z} \right)|z = 0,\ C_{fy} = \frac{\mu_{hnf}}{\rho_f u_w^2}\left(\frac{\partial v}{\partial z} \right)|z = 0,$$
$$\quad (12)$$

$$Nu_x = \frac{-k_{hnf}(\partial T/\partial z)_{z=0} + (q_r)_{z=0}}{k_f(T_w - T_\infty)}.$$

Substituting (7) into (12) yields

TABLE 1: Thermophysical features of hybrid nanofluid [32–34].

Properties	Hybrid nanofluid
Dynamic viscosity	$\mu_{hnf} = \mu_f/(1 - \phi_{Cu})^{2.5}(1 - \phi_{Al_2O_3})^{2.5}$
Density	$\rho_{hnf} = (1 - \phi_{Cu})[(1 - \phi_{Al_2O_3})\rho_f + \phi_{Al_2O_3}\rho_{Al_2O_3}] + \phi_{Cu}\rho_{Cu}$
Thermal conductivity	$k_{hnf} = k_{Cu} + 2k_{nf} - 2\phi_{Cu}(k_{nf} - k_{Cu})/k_{Cu} + 2k_{nf} + \phi_{Cu}(k_{nf} - k_{Cu}) \times (k_{nf})$ where $k_{nf} = k_{Al_2O_3} + 2k_f - 2\phi_{Al_2O_3}(k_f - k_{Al_2O_3})/k_{Al_2O_3} + 2k_f + \phi_{Al_2O_3}(k_f - k_{Al_2O_3}) \times (k_f)$
Heat capacity	$(\rho c_p)_{hnf} = (1 - \phi_{Cu})[(1 - \phi_{Al_2O_3})(\rho c_p)_f + \phi_{Al_2O_3}(\rho c_p)_{Al_2O_3}] + \phi_{Cu}(\rho c_p)_{Cu}$
Electrical conductivity	$\sigma_{hnf} = \sigma_{Cu} + 2\sigma_{nf} - 2\phi_{Cu}(\sigma_{nf} - \sigma_{Cu})/\sigma_{Cu} + 2\sigma_{nf} + \phi_{Cu}(\sigma_{nf} - \sigma_{Cu}) \times (\sigma_{nf})$ where $\sigma_{nf} = \sigma_{Al_2O_3} + 2\sigma_f - 2\phi_{Al_2O_3}(\sigma_f - \sigma_{Al_2O_3})/\sigma_{Al_2O_3} + 2\sigma_f + \phi_{Al_2O_3}(\sigma_f - \sigma_{Al_2O_3}) \times (\sigma_f)$

TABLE 2: The thermophysical properties [32–34].

Properties	Water (H_2O)	Copper (Cu)	Alumina (Al_2O_3)
$\rho\,(kg/m3)$	997.1	8933	3970
$c_p\,(J/kg\,K)$	4179	385	765
$k\,(W/m\,K)$	0.613	400	40
$\sigma\,(S/m)$	0.05	5.96×10^7	3.69×10^7
Pr	6.2		

$$\sqrt{Re}C_{fx} = \frac{1}{\xi_2}f''(0); \sqrt{Re}C_{fy} = \frac{1}{\xi_2}g'(0) \quad \sqrt{\frac{Re}{2}}Nu_x$$
$$= -\left(\frac{k_{hnf}}{k_f} + \frac{4}{3}R\,d\right)\theta'(0), \tag{13}$$

where Re_x is the local Reynolds number.

3. Stability Analysis

Two branches of solution against the involved parameters are observed. In order to inspect the branch of solution with more physical relevance, the stability analysis has been performed for both branches. The governing equations (2)-(5) with unsteady form are

$$u_t + uu_x + vu_y + wu_z - 2\widetilde{\Omega}v = -\frac{P_x}{\rho_{hnf}} + \frac{\mu_{hnf}}{\rho_{hnf}}[u_{xx} + u_{yy} + u_{zz}] - \frac{\sigma_{hnf}}{\rho_{hnf}}B^2 u, \tag{14}$$

$$v_t + uv_x + vv_y + wv_z + 2\widetilde{\Omega}u = -\frac{P_y}{\rho_{hnf}} + \frac{\mu_{hnf}}{\rho_{hnf}}[v_{xx} + v_{yy} + v_{zz}]v - \frac{\sigma_{hnf}}{\rho_{hnf}}B^2 v, \tag{15}$$

$$w_t + uw_x + vw_y + ww_z = -\frac{P_z}{\rho_{hnf}} + \frac{\mu_{hnf}}{\rho_{hnf}}[w_{xx} + w_{yy} + w_{zz}], \tag{16}$$

$$(\rho c_p)_{hnf}[T_t + uT_x + vT_y + wT_z] = k_{hnf}[T_{xx} + T_{yy} + T_{zz}]T - q_{r\,z} + Q_0(T - T_\infty). \tag{17}$$

The unsteady similarity solution can be considered as follows [33–35]:

$$\begin{cases} u = cx^n f_\eta(\eta, \tau), v = cx^n g(\eta, \tau), \\ w = -\sqrt{\frac{c\vartheta_f(n+1)}{2}}x^{(n-1)/2}\left[f(\eta, \tau) + \frac{n-1}{n+1}\eta f_\eta(\eta, \tau) - \frac{2\tau}{n+1}\eta f(\eta, \tau)\right], \\ \theta(\eta, \tau) = ((T - T_\infty)/(T_w - T_\infty)). \end{cases} \tag{18}$$

where the η is the same as in equation (7) and the dimensionless time is the $\tau = ctx^{n-1}$, where the subscription represents the derivative of the variable subscripted. Remember that continuity (1) is also satisfied by the values u, v, and w given above. Equation (18) is substituted into equations (14)-(17), and one can get

$$f_{\eta\eta\eta} + \xi_1\xi_2\left[ff_{\eta\eta} - \frac{2n}{(n+1)}(f_\eta)^2 + \frac{4\Omega}{(n+1)}g\right.$$
$$\left. + \frac{2(n-1)}{(n+1)}\tau(f_\tau f_{\eta\eta} - f_\eta f_{\tau\eta}) - \frac{2}{(n+1)}f_{\tau\eta}\right] \tag{19}$$

$$g_{\eta\eta} + \xi_1\xi_2\left[fg_\eta - \frac{2n}{(n+1)}f_\eta g - \frac{4\Omega}{(n+1)}f_\eta\right.$$
$$\left. + \frac{2(n-1)}{(n+1)}\tau(f_\tau g_\eta - g_\tau f_\eta) - \frac{2}{(n+1)}g_\tau\right] \tag{20}$$
$$- \frac{2}{(n+1)}\frac{\sigma_{hnf}}{\sigma_f}\xi_2 Mg = 0,$$

$$\frac{\xi_3}{Pr}\left(\frac{k_{hnf}}{k_f} + \frac{4}{3}R\,d\right)\theta_{\eta\eta} + \theta_\eta f + \xi_3 Q\theta$$
$$+ 2\tau\left(f_\tau\theta_\eta - \theta_\tau f_\eta\right) - \theta_\tau = 0, \tag{21}$$

subject to BCs,

$$\begin{cases} f(0,\tau) = -b\sqrt{\dfrac{2}{n+1}}, \, f'(0,\tau) = \lambda, \, g(0,\tau) = 0, \theta(0,\tau) = 1 \\[2mm] f'(\eta,\tau) \longrightarrow 0, g(\eta,\tau) \longrightarrow 0\,\theta(\eta,\tau) \longrightarrow 0, \, as\,\eta \longrightarrow \infty \end{cases}. \tag{22}$$

It is assumed that [28]

$$f(\eta,\tau) = f_0(\eta) + e^{-\varepsilon\tau}F(\eta,\tau), g(\eta,\tau).$$
$$= g_0(\eta) + e^{-\varepsilon\tau}G(\eta,\tau), \, \theta(\eta,\tau) = \theta_0(\eta) + e^{-\varepsilon\tau}H(\eta,\tau). \tag{23}$$

The solution associated to the formulated equations (8)–(10) with boundary conditions (11) is denoted with $f_0(\eta)$, $g_0(\eta)$, and $\theta_0(\eta)$. The decay and growth disturbance rate is defined with ε. It is assumed that (η,τ), $G(\eta,\tau)$, and $H(\eta,\tau)$ and derivatives of these expressions are smaller in contrast to the steady state situation. Such assumptions are followed due to the linear stability of flow pattern. Upon replacing equation (26) into set of expressions (19)–(21) with taking $= 0, F(\eta,\tau)$, $G(\eta,\tau)$, and $H(\eta,\tau)$ are associated to $F_0(\eta)$, $G_0(\eta)$, and $H_0(\eta)$. On this end, the linear eigenvalue problem is formulated as

$$F_0''' + \xi_1\xi_2\left\{f_0 F_0'' + F_0 f_0'' + \frac{2}{n+1}(\varepsilon - 2nf_0')F_0' + \frac{4\Omega}{(n+1)}G_0\right\}$$
$$- \frac{2}{(n+1)}\frac{\sigma_{hnf}}{\sigma_f}\xi_2 MF_0' = 0, \tag{24}$$

$$G_0'' + \xi_1\xi_2\left[g_0'F_0 + G_0'f_0 - \frac{2n}{(n+1)}(f_0'G_0 + F_0'g_0)\right.$$
$$\left. - \frac{4\Omega}{(n+1)}F_0' + \frac{2}{(n+1)}\varepsilon G_0\right] - \frac{2}{(n+1)}M\frac{\sigma_{hnf}}{\sigma_f}\xi_2 G_0 = 0, \tag{25}$$

$$\frac{\xi_3}{Pr}\left(\frac{k_{hnf}}{k_f} + \frac{4}{3}R\,d\right)H_0'' + \theta_0'F_0 + H_0'f_0 + \xi_3 QH_0 + \varepsilon H_0 = 0, \tag{26}$$

with

$$\begin{cases} F_0(0) = 0, F_0'(0) = 0, G_0(0) = 0, H_0(0) = 0 \\[2mm] F_0'(\eta) \longrightarrow 0, G_0(\eta) \longrightarrow 0\,H_0(\eta) \longrightarrow 0, \, as\,\eta \longrightarrow \infty \end{cases}. \tag{27}$$

We can solve equations (24)–(26) along with BCs (27) by using the numerical values of $f_0(\eta)$, $g_0(\eta)$, and $\theta_0(\eta)$ which were obtained from the solutions of equations (8)–(10) with

Table 3: Values of $\sqrt{Re}C_{fx}$ and $\sqrt{Re}C_{fy}$ for several values of Ω when $\lambda = 1, \phi_{Al_2O_3} = \phi_{Cu} = 0, b = 0, n = 1$.

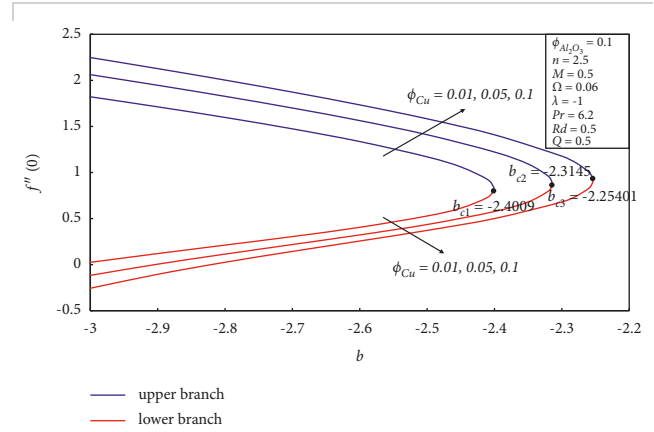|	$\sqrt{Re}C_{fx}$		$\sqrt{Re}C_{fy}$	
Ω	[35]	Present results	[28]	Present results
0	−1.0000	−1.0000625	0.0000	0.0000000
0.5	−1.1384	−1.1383806	−0.5128	−0.5127602
1	−1.3250	−1.3250287	−0.8371	−0.8370983
2	−1.6523	−1.6523520	−1.2873	−1.2872588
3	−1.9289	−1.9289315	−1.6248	−1.6247357
4	−2.1716	−2.1715931	−1.9054	−1.9053929
5	−2.3901	−2.3901398	−2.1506	−2.1505265

Figure 2: Impact of b on $f''(0)$ for fixed values of ϕ_{Cu}.

BCs (11). It is worth noting that the homogeneous linear equations (24)–(26) subject to constants (27) construct an eigenvalue system with eigenvalue ε. By solving equations (24)–(27), a set of eigenvalues $\varepsilon_1 < \varepsilon_2 < \varepsilon_3 < \ldots$ is obtained.

4. Results and Discussion

Following to the investigation of Devi and Devi [33, 34] and Lund et al. [35], here water is considered as base material with copper (Cu) and aluminum nanoparticles (Al_2O_3). Moreover, volume fraction of aluminum is kept constant against the variation of copper volume oxide ($0.01 \leq \phi_{Cu} \leq 0.1$). The comparison validation for ensuring the validity task has been done in Table 3 with work of Zaimi et al. [37] with excellent comparison results.

Figures 2–4 are sketched to observe the physical aspect of ϕ_{Cu} on $f''(0)$, $g'(0)$, and $-\theta\prime(0)$. Results are visualized for suction case. The dual branches of solution are results for various values of suction case. The critical points for $\phi_{Cu} = 0.01$ are $b_{c1} = -2.4009$ while $b_{c2} = -2.3145$ and $b_{c3} = -2.25401$ are the critical points against $\phi_{Cu} = 0.05$ and $\phi_{Cu} = 0.01$, respectively. Two different categories of branches such as dual branch ($b \leq b_{ci}$) and no branch ($b > b_{ci}$) for suction parameter b exist. Moreover, larger change in ϕ_{Cu} results increment in b_{ci} which preserve a separation. The dominant values of suction do not allow tension in moving particles, and vorticity is not smothered. In upper branch, with larger suction, the decrement in wall shear force and heat transfer rate is noted. In lower branch, the heat transfer rate is lower but wall shear force
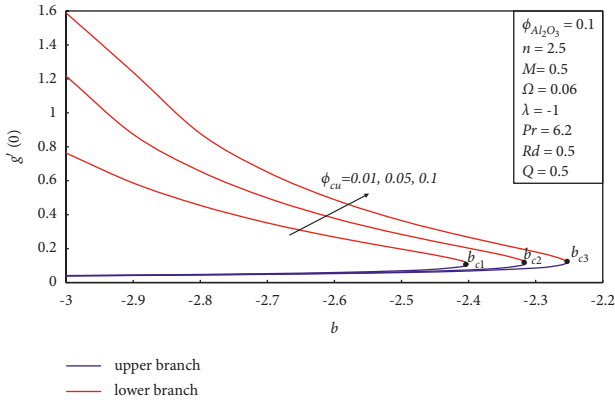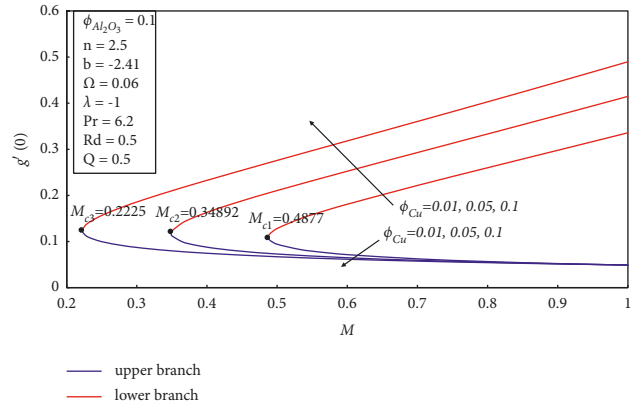
FIGURE 3: Impact of b on $g'(0)$ for fixed values of ϕ_{Cu}.
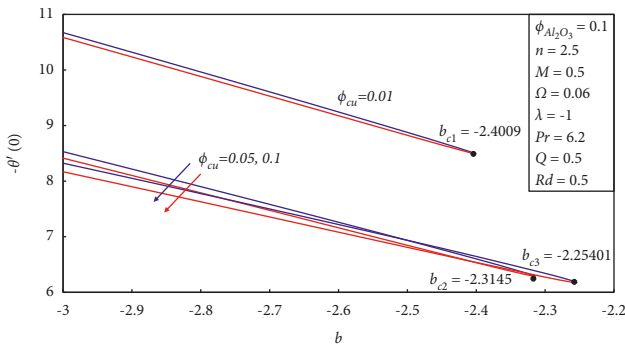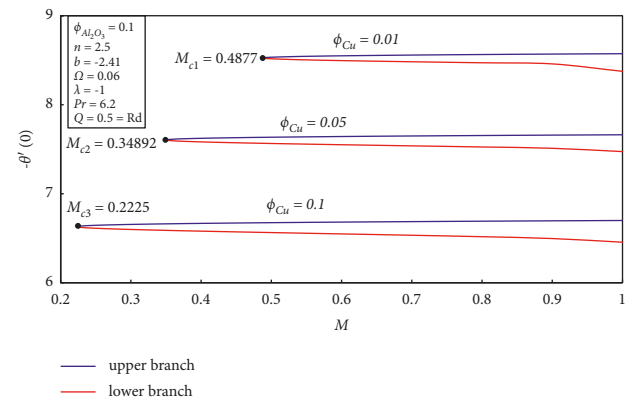

FIGURE 4: Impact of b on $-\theta'(0)$ for fixed values of ϕ_{Cu}.

FIGURE 5: Impact of M on $f''(0)$ for fixed values of ϕ_{Cu}.

FIGURE 6: Impact of M on $g'(0)$ for fixed values of ϕ_{Cu}.

FIGURE 7: Impact of M on $-\theta'(0)$ for fixed values of ϕ_{Cu}.
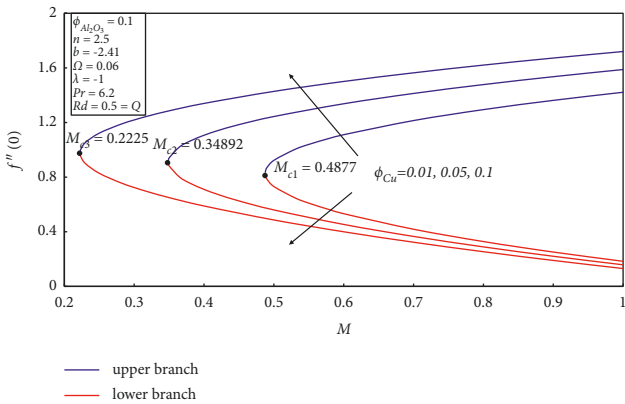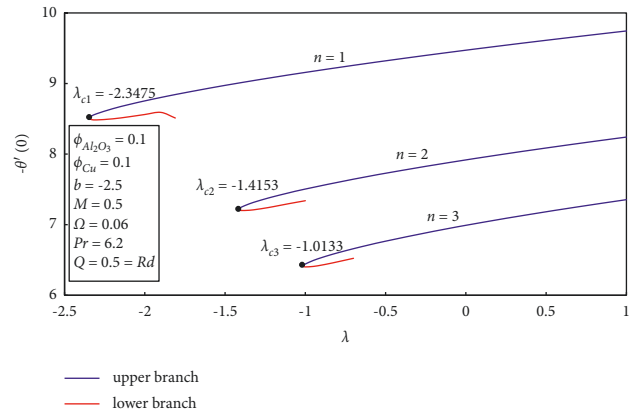

FIGURE 8: Impact of λ on $-\theta'(0)$ for fixed values of n.

enhanced. In upper branch, no significant change in $g'(0)$ due to suction parameter is inspected while in lower branch, $g'(0)$ declined.

Figures 5–7 show the variation of $''(0)$, $g'(0)$ and $-\theta'(0)$ magnetic parameter M against copper solid volume fraction ϕ_{Cu}. As ϕ_{Cu} grows, the critical point of M_c shifts to the left, assisting in the separation of the boundary layer. $M_{c1} = 0.4877$, $M_{c2} = 0.34892$, and $M_{c3} = 0.2225$ referred to critical points of M for $\phi_{Cu} = 0.01$, 0.05, and 0.1. As a result, the dual-branch representation is possible for $M \geq M_{ci}$ where $i = 1, 2, 3$; however, no branch exists for $M < M_{ci}$. The variation in $f''(0)$ and $-\theta'(0)$ get dominant change

against ϕ_{Cu} in the upper branch for a fixed value of M, while the reversal phenomenon can be seen in the bottom branch. Furthermore, as the magnetic field is increased, the skin friction coefficient $g'(0)$ decreases by maintaining constant values of ϕ_{Cu} in the upper branch while slower trend is predicted in the lower branch.

The influences of positive constant n on $f''(0)$, $g'(0)$, and $-\theta'(0)$ is reported in Figures 8 and 9The obtained results are prepared in view of stretching/shrinking parameter (λ). A lower observation of $f''(0)$for stretching constant is noted. In
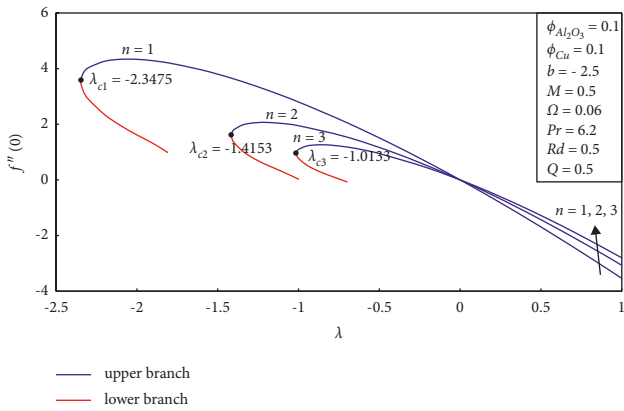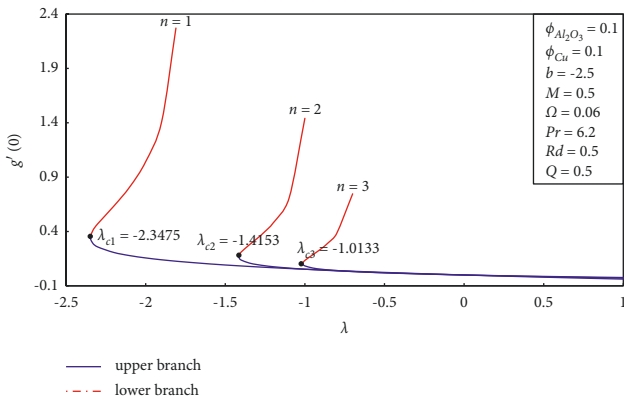
FIGURE 9: Impact of λ on $f''(0)$ for fixed values of n.

FIGURE 10: Impact of λ on $g'(0)$ for fixed values of n.
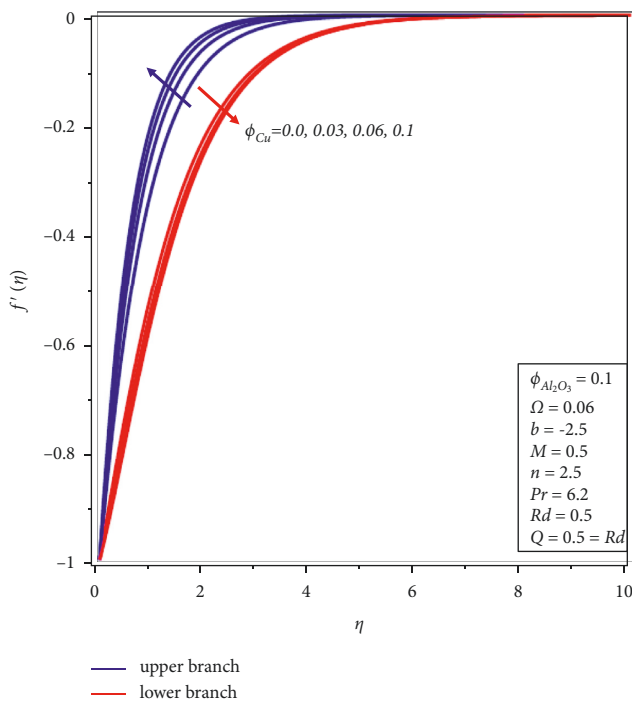

FIGURE 11: Variation of $f'(\eta)$ against η for various values of ϕ_{Cu}.

FIGURE 12: Variation of $g(\eta)$ against η for various values of ϕ_{Cu}.
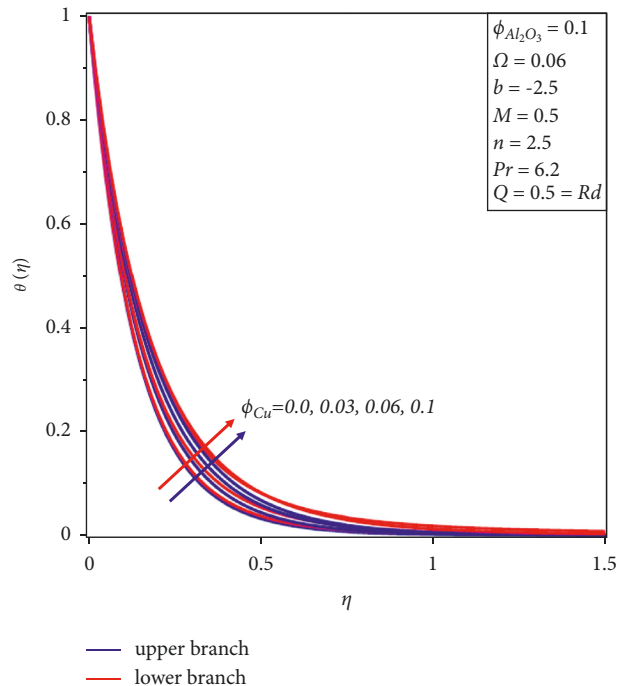
FIGURE 13: Variation of $\theta(\eta)$ against η for various values of ϕ_{Cu}.

upper zone, upon increasing λ, the change in $g'(0)$ is declining while $g'(0)$ increases. The thermal boundary layer separation is greater for linear stretching as compared to nonlinear case. Moreover, the heat transfer rate for stretching case is more progressive as compared to shrinking case. From Figure 10, a declining change in $f''(0)$ is observed for greater λ.

Figures 11–13 show the effect of copper solid volume fraction ϕ_{Cu} on velocity profiles $f'(\eta)$ and $g(\eta)$ in the x-
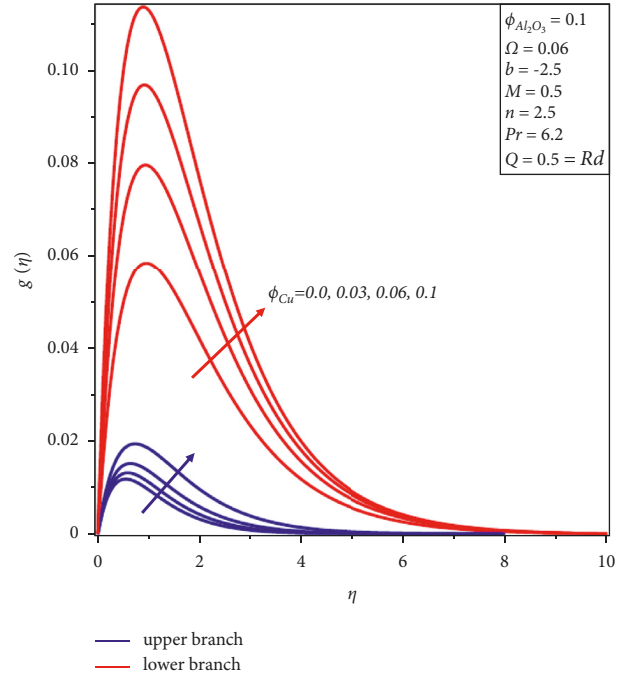
FIGURE 14: Variation of $g(\eta)$ against η for various values of Ω.

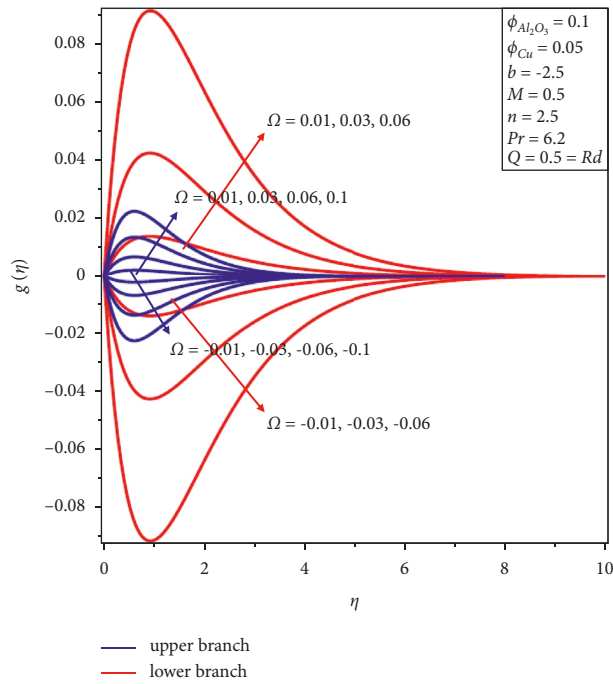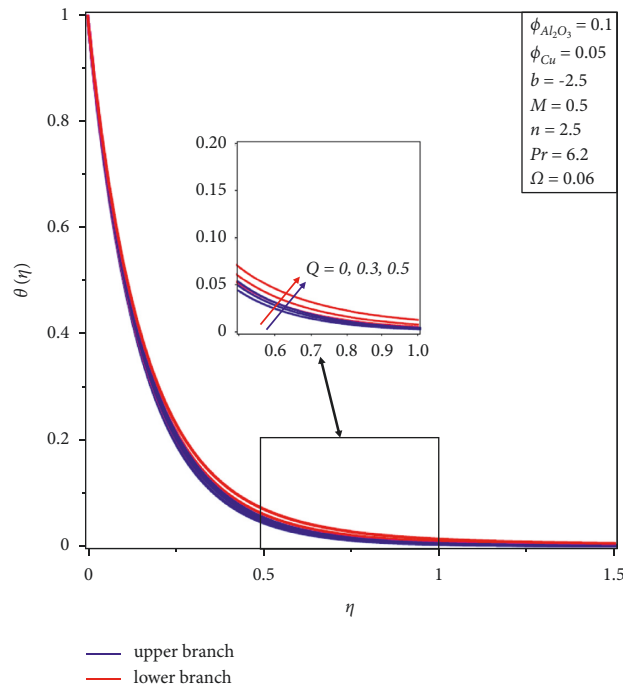FIGURE 15: Variation of $\theta(\eta)$ against η for various values of Q.

and y-directions, as well as a temperature profile $\theta(\eta)$. Different profiles in both branches fulfill the far-field BCs $\eta \longrightarrow \infty$ for various values of ϕ_{Cu} and hence validate the obtained numerical results. In Figure 11, the field of velocity decreases as parameter ϕ_{Cu} increases in the upper surface while contradictory results are noted in the lower branch. This is because the volume fraction slows the velocity of the fluid, which reduces the thickness of the momentum layer

and, as a result, the velocities in the x-direction. On the other hand, when ϕ_{Cu} rises, velocity rate increases in the y-direction for both branches (refer to Figure 12). Furthermore, as expected, heat transfer rate gets arisen for copper solid volume percentage ϕ_{Cu} rises in both branches.

The graphical outcomes for rotation constant Ω parameter on velocity along y-directions ($g(\eta)$) have been worked out in Figure 14. The solution has a symmetrical nature. When the

TABLE 4: The values of ε_1 for various values of ϕ_{Cu} and b when $\lambda = -1$, $M = 0.5$, $n = 2.5$, $Pr = 6.2$, $R\,d = Q = 0.5$.

ϕ_{Cu}	b	ε_1	
		Upper branch	Lower branch
0.01	−3	2.2281	−2.2827
	−2.5	1.9924	−1.9001
0.03	−3	2.6295	−2.8547
	−2.5	2.1824	−2.4373
0.05	−3	2.8626	−3.0626
	−2.5	2.25463	−2.4515
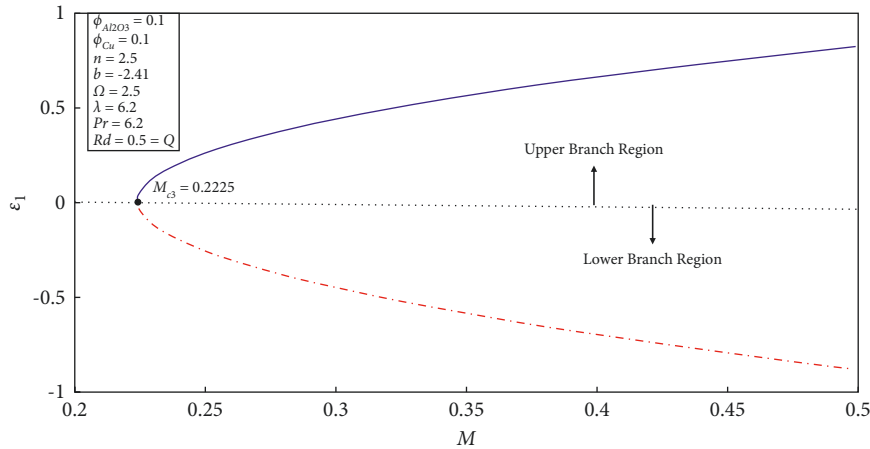
FIGURE 16: The values of ε_1 for various values of M.

value of Ω is positive, velocity increases in both branches. When the value of Ω is negative, the velocity of the hybrid nanofluid decreases. It is also discovered that when $-0.06 \leq \Omega \leq 0.06$, two branches are possible. Figure 15 shows the effect of heat sink/source parameter on temperature profiles. It has been observed that temperature of hybrid nanofluid increases in both solutions when the parameter Q increases. This enhancement is due to external heat source. This aids in the formation of the thermal boundary layer thickness.

It is well justified fact that upon existing of different solution branches, the importance of stability analysis cannot be denied identifying the more realistically branch. Usually, the upper branch is referred to the physical branch as it meets with the boundary assumptions. However, the stability of lower branch is also importance and can be observed via stability procedure. After carefully noticing, it is claimed that upper branch is more stable in view of ε_1. The positive sign of ε_1 ensures that stability of branch and reflects the decay and growth results. The negative values of ε_1 show that the branch is unstable. Both positive and negative values of ε_1 upper and lower branches are presented via Table 4. Figure 16 shows the lower numerical values of eigenvalue for upper and lower surface branches.

5. Conclusions

In a rotating hybrid nanofluid, the laminar steady boundary flow on a stretching/shrinking sheet was investigated. The governing PDEs were numerically solved in *bvp4c* using the well-known collocation approach known as the 3-stage-Lobatto-3a method. Numerical results for various values of physical application parameters have been graphically presented and thoroughly analyzed. The values of $\sqrt{Re}C_{fx}$ and $\sqrt{Re}C_{fy}$ are compared to published publications in order to validate the obtained numerical results, which show a positive agreement. In the precise range of the magnetic, suction, and shrinking/stretching parameters, dual branches have been discovered. The following are a few key points from the current study:

(i) For suction case, the heat transfer rate is larger as compared to injection phenomenon in the upper branch.

(ii) In upper branch, no significance change in y-directional velocity is observed while declining change in velocity is noticed for lower branch.

(iii) The presence of external heat source enhanced the heat transfer rate in both branches. However, the increment in heat transfer is relatively larger in the upper branch.

(iv) No dual branches exist outside the magnetic parameter and stretching/shrinking constant.

(v) Upon increasing the copper nanoparticle volume fraction, the enhancement in temperature rate is measured.

(vi) The fluctuation in thermal boundary layer is more progressive for linear stretching instead of nonlinear case.

Nomenclature

Al_2O_3:	Alumina
T_∞:	Ambient temperature
Cu:	Copper
f', g:	Dimensionless velocity
M:	Hartmann number
b:	Injunction/suction parameter
N_{ux}:	Local Nusselt number
Re_x:	Local Reynolds number
B:	Magnetic field
$w_w(x)\ (m/s)$:	Mass flux of velocity
Pr:	Prandtl number
C_{fx}, C_{fy}:	Skin friction coefficient
$T:(K)$:	Temperature
Q:	Sink/source parameter
T_w:	Variable temperature at the sheet
u, v, w:	(m/s) Velocity components
$u_w(x)\ (m/s)$:	Velocity of surface
H_2O:	Water
$\tilde{\Omega}$:	Angular velocity
ρ_{hnf}:	Density
θ:	Dimensionless temperature
μ_{hnf}:	Dynamic viscosity
σ_{hnf}:	Electrical conductivity
$(c_p)_{hnf}$:	Heat capacity
ε_1:	Smallest eigenvalue
τ:	Stability transformed variable
λ:	Stretching/shrinking parameter
k_{hnf}:	Thermal conductivity,
η:	Transformed variable
ε:	Unknown eigenvalue.

Data Availability

All data are given in the paper.

Conflicts of Interest

The authors declare that they have no conflicts of interest.

References

[1] S. U. Choi, *Enhancing thermal Conductivity of Fluids with Nanoparticles (No. ANL/MSD/CP-84938*, Argonne National Lab, IL (United States), 1995.

[2] M. Turkyilmazoglu, "Fully developed slip flow in a concentric annuli via single and dual phase nanofluids models," *Computer Methods and Programs in Biomedicine*, vol. 179, Article ID 104997, 2019.

[3] M. K. Nayak, I. S. Oyelakin, A. J. Chamkha, S. 4 Mondal, and P. Sibanda, "Three-dimensional rotating flow of an Oldroyd-B nanofluid with relaxation-retardation viscous dissipation," *Journal of Nanofluids*, vol. 10, pp. 408–419, 2021.

[4] M. d. F. M. d. Basir, M. Bilal, R. Choudhary, J. Mackolil, B. Mahanthesh, and K. S. Nisar, "Numerical and Sensitivity Analysis of MHD Bioconvective Slip Flow of Nanomaterial with Binary Chemical Reaction and Newtonian heating," *Heat Transfer Asian Research*, vol. 50, pp. 5439–5466, 2021.

[5] S. Ahmad, M. N. Khan, S. Nadeem, A. Rehman, H. Ahmad, and R. Ali, "Impact of Joule Heating and Multiple Slips on a Maxwell Nanofluid Flow Past a Slendering Surface," *Communications in Theoretical Physics*, vol. 74, no. (1), 2021.

[6] S. Nadeem, W. Fuzhang, F. M. Alharbi et al., "Numerical computations for Buongiorno nano fluid model on the boundary layer flow of viscoelastic fluid towards a nonlinear stretching sheet," *Alexandria Engineering Journal*, vol. 61, pp. 1769–1778, 2022.

[7] H. Vaidya, K. V. P. I. Tlili, O. D. Makinde et al., "Mixed convective nanofluid flow over a non linearly stretched Riga plate," *Case Studies in Thermal Engineering*, vol. 24, Article ID 100828, 2021.

[8] H. Wang, M. Pang, Y. Diao, and Y. Zhao, "Heat transfer characteristics and flow features of nanofluids in parallel flat minichannels," *Powder Technology*, vol. 402, Article ID 117321, 2022.

[9] A. H. Abdelaziz, W. M. E. l. Maghlany, A. A. E. l. Din, and M. A. Alnakeeb, "Mixed convection heat transfer utilizing Nanofluids ionic Nanofluids and hybrid nanofluids in a horizontal tube," *Alexandria Engineering Journal*, vol. 61, pp. 9495–9508, 2022.

[10] A. S. Sabu, A. Wakif, S. Areekara, A. Mathew, and N. A. Shah, "Significance of nanoparticles' shape and thermo-hydrodynamic slip constraints on MHD alumina-water nanoliquid flows over a rotating heated disk," *The passive control approach, International Communications in Heat and Mass Transfer*, vol. 129, Article ID 105711, 2021.

[11] O. Ojjela, O. Ojjela, P. K. Kambhatla, and F. Mebarek-Oudina, "Shape effect of MoS$$_2$$ nanoparticles on entropy generation and heat transport in viscoelastic boundary layer flow," *Pramana*, vol. 95, no. 4, p. 182, 2021.

[12] J. Dong, Q. Zheng, C. Xiong, E. Sun, and J. Chen, "Experimental investigation and application of stability and thermal characteristics of SiO2-ethylene-glycol/water nanofluids," *International Journal of Thermal Sciences*, vol. Volume 176, Article ID 107533, 2022.

[13] S. Sivasankaran and M. Bhuvaneswari, "Numerical study on influence of water based hybrid nanofluid and porous media on heat transfer and pressure loss," *Case Studies in Thermal Engineering*, vol. 34, Article ID 102022, 2022.

[14] N. Acharya, "Finite element analysis on the hydrothermal pattern of radiative natural convective nanofluid flow inside a square enclosure having nonuniform heated walls," *Heat Transfer Asian Research*, vol. 51, no. 1, pp. 323–354, 2022.

[15] H. Mondal and P. K. Kundu, "Spectral approach to study the entropy generation of radiative mixed convective couple stress fluid flow over a permeable stretching cylinder," *Part C: Journal of Mechanical Engineering Science*, vol. 235, no. 15, 2021.

[16] N. Acharya, "Spectral simulation to investigate the effects of active passive controls of nanoparticles on the radiative nanofluidic transport over a spinning disk," *J. Thermal Sci. Eng. Appl*, vol. 13, no. 3, Article ID 031023, 2021.

[17] A. Shafiq, S. A. Lone, T. N. Sindhu, Q. M. A. l. Mdallal, and G. Rasool, "Statistical modeling for bioconvective tangent hyperbolic nanofluid towards stretching surface with zero mass flux condition," *Scientific Reports*, vol. 11, Article ID 13869, (2021).

[18] T. Hayat, A. Shafiq, and A. Alsaedi, "Effect of Joule heating and thermal radiation in flow of third grade fluid over radiative surface," *PLoS One*, vol. 9, no. 1, 2014.

[19] S. Ahmad, M. Ashraf, and K. Ali, "Bioconvection due to gyrotactic microbes in a nanofluid flow through a porous medium," *Heliyon*, vol. 6, Article ID e05832, 2020.

[20] U. Nazir, M. Sohail, M. B. Hafeez, M. Krawczuk, S. Askar, and S. Wasif, "An inclination in thermal energy using nanoparticles with casson liquid past an expanding porous surface," *Energies*, vol. 14, no. 21, p. 7328, 2021.

[21] B. Mahanthesh, N. S. Shashikumar, B. J. Gireesha, and I. L. Animasaun, "Effectiveness of Hall current and exponential heat source on unsteady heat transport of dusty TiO2-EO nanoliquid with nonlinear radiative heat," *Journal of Computational Design and Engineering*, vol. 6, pp. 551–561, 2019.

[22] Kh. Hosseinzadeh, So. Roghani, A. R. Mogharrebi, A. Asadi, M. Waqas, and D. D. Ganji, "Investigation of cross-fluid flow containing motile gyrotactic microorganisms and nanoparticles over a three-dimensional cylinder," *Alexandria Engineering Journal*, vol. 59, no. 5, pp. 3297–3307, Oct. 2020.

[23] T. Armaghani, M. S. Sadeghi, A. M. Rashad et al., "MHD mixed convection of localized heat source/sink in an Al_2O_3-Cu/water hybrid nanofluid in L-shaped cavity," *Alexandria Engineering Journal*, vol. 60, pp. 2947–2962, 2021.

[24] T. N. Sindhu and A. Atangana, "Reliability analysis incorporating exponentiated invers," *Weibull distribution and inverse power law*, vol. 37, no. 6, pp. 2399–2422, 2021.

[25] G. Sowmya, B. J. Gireesha, I. L. Animasaun, and N. A. Shah, "Significance of buoyancy and Lorentz forces on water-conveying iron(III) oxide and silver nanoparticles in a rectangular cavity mounted with two heated fins: heat transfer analysis," *Journal of Thermal Analysis and Calorimetry*, vol. 144, pp. 2369–2384, (2021.

[26] L. S. Sundar, V. Punnaiah, M. K. Singh, A. M. B. Pereira, and A. C. M. Sousa, "Solar energy absorbed thermosyphon flat plate collector analysis using Cu/H_2O nanofluid – an experimental study," *Energy and Climate Change*, vol. Volume 2, Article ID 100028, 2021.

[27] S. Akhtar, L. B. McCash, S. Nadeem, S. Saleem, and A. Issakhov, "Convective heat transfer for Peristaltic flow of SWCNT inside a sinusoidal elliptic duct," *Science Progress*, vol. 104, no. 2, pp. 1–17, 2021.

[28] M. R. Eid and F. Mabood, "Entropy analysis of a hydromagnetic micropolar dusty carbon NTs-kerosene nanofluid with heat generation: Darcy–Forchheimer scheme," *Journal of Thermal Analysis and Calorimetry*, 2020.

[29] A. Shahid, M. M. Bhatti, O. A. Bég, I. L. Animasaun, and K. Javid, "Spectral computation of reactive bi-directional hydromagnetic non-Newtonian convection flow from a stretching upper parabolic surface in non-Darcyporous medium," *International Journal of Modern Physics B*, vol. 35, Article ID 2150294, (2021).

[30] J. K. Madhukesh, R. Naveen Kumar, R. J. Punith Gowda et al., "Numerical simulation of AA7072-AA7075/water-based hybrid nanofluid flow over a curved stretching sheet with Newtonian heating: a non-Fourier heat flux model approach," *Journal of Molecular Liquids*, vol. 335, p. 116103, 2021.

[31] N. Acharya, "On the flow patterns and thermal control of radiative natural convective hybrid nanofluid flow inside a square enclosure having various shaped multiple heated obstacles," *The European Physical Journal Plus*, vol. 136, p. 889, 2021.

[32] S. A. Devi and S. S. Devi, "Numerical investigation of hydromagnetic hybrid Cu–Al2O3/water nanofluid flow over a permeable stretching sheet with suction," *Int J of Nonl Sci and Numerical Simulation*, vol. 17, no. 5, pp. 249–257, 2016.

[33] S. S. Devi and S. A. Devi, "Numerical investigation of three-dimensional hybrid Cu–Al2O3/water nanofluid flow over a stretching sheet with effecting Lorentz force subject to Newtonian heating," *Canadian Journal of Physics*, vol. 94, no. 5, pp. 490–496, 2016.

[34] L. A. Lund, Z. Omar, and I. Khan, "Darcy-Forchheimer porous medium effect on rotating hybrid nanofluid on a linear shrinking/stretching sheet," *International Journal of Numerical Methods for Heat and Fluid Flow*, 2021.

[35] Y. Y. Teh and A. Ashgar, "Three dimensional MHD hybrid nanofluid flow with rotating stretching/shrinking sheet and Joule heating," *CFD Letters*, vol. 13, no. 8, pp. 1–19, 2021.

[36] K. Zaimi, A. Ishak, and I. Pop, "Stretching surface in rotating viscoelastic fluid," *Applied Mathematics and Mechanics*, vol. 34, no. 8, pp. 945–952, 2013.

[37] S. Ahmad, S. Nadeem, and Rehman, "Aysha; mathematical analysis of thermal energy distribution in a hybridized mixed convective flow," *Journal of Nanofluids*, vol. 10, no. 2, pp. 222–231, 2021.